

***Ab initio* calculations and ellipsometry measurements of the optical properties of the layered semiconductor In_4Se_3**

L. Makinistian,^{1,*} E. A. Albanesi,¹ N. V. Gonzalez Lemus,¹ A. G. Petukhov,² D. Schmidt,³ E. Schubert,³ M. Schubert,³ Ya. B. Losovyj,⁴ P. Galiy,⁵ and P. Dowben⁶

¹*INTEC-CONICET, Güemes 3450, 3000 Santa Fe, Argentina and Facultad de Ingeniería, Universidad Nacional de Entre Ríos, 3101 Oro Verde (ER), Argentina*

²*Department of Physics, South Dakota School of Mines, Rapid City, South Dakota 57701, USA*

³*Department of Electrical Engineering and Nebraska Center for Materials and Nanoscience, University of Nebraska, Lincoln, Nebraska 68588, USA*

⁴*Center for Advanced Microstructures and Devices, Louisiana State University, Baton Rouge, Louisiana 70806, USA*

⁵*Electronics Department, Ivan Franko National University of Lviv, 50 Dragomanov Str., 79005 Lviv, Ukraine*

⁶*Department of Physics and Astronomy and the Nebraska Center for Material and Nanoscience, University of Nebraska, Lincoln, Nebraska 68588, USA*

(Received 5 October 2009; revised manuscript received 17 December 2009; published 26 February 2010)

In this work, we present a thorough study of the optical properties of the layered orthorhombic compound In_4Se_3 . The dielectric function—real and imaginary parts, the complex refractive index, the reflectivity, the absorption coefficient, and the conductivity of In_4Se_3 were calculated with the inclusion of the spin-orbit interaction, using an *ab initio* FP-LAPW method based on DFT. Also, generalized ellipsometry was employed for more precise measurement of the anisotropic dielectric functions for polarization along crystal *a*, *b*, and *c* axes of orthorhombic absorbing In_4Se_3 single crystals cut approximately parallel to (100) at photon energies from 0.76 to 3.1 eV. Our experimental results show a good agreement with our calculations. We discuss the location and nature of the main optical peaks appearing in the spectra. The obtained optical functions display a rather anisotropic behavior, mainly in the infrared-visible region. Our results seem to be predictive to a high extension, given the scarce experimental information about its optical properties.

DOI: [10.1103/PhysRevB.81.075217](https://doi.org/10.1103/PhysRevB.81.075217)

PACS number(s): 71.20.-b, 78.20.Ci, 71.15.Mb

I. INTRODUCTION

The In_4Se_3 orthorhombic crystal (D_{2h}^{12}) is a narrow band gap semiconductor containing 27 atoms in the unit cell (see Fig. 1) and much is known about its band structure. It crystallizes in a layered structure with, in principle, weak interaction of the van der Waals type between the layers and strong covalent-ionic interactions within the layers.¹

The material seems to have been less studied among the layered chalcogenides crystals,^{2,3} yet continues to attract attention as a natural low dimensional quasi-two-dimensional (quasi-2D) material in much the same way as occurs with layered systems with flat layers held together with van der Waals forces. Indeed, it was suggested that it could be suitable for fabrication of infrared optical fiber⁴ and nanowires,⁵ and a recent article reports an In_4Se_3 -related material (In_4Se_3 self-doped with Se deficiencies) with a high thermoelectric performance as an important candidate for recycling waste heat into useful electricity.⁶ In addition, In_4Se_3 polycrystalline thin films have been synthesized and suggested for photovoltaic applications.^{7,8}

Also, other experimental [e.g., Auger spectroscopy,⁹ and single crystal surface characterization with STM, LEED, and XPS (Ref. 3)] and theoretical (e.g., lattice dynamics modelization,¹⁰ pseudopotential band structure calculations¹¹) studies have been reported. In previous work,¹²⁻¹⁴ we studied both the surface and the bulk electronic states, showing that the system does have a bulk band structure (i.e., discernable and significant band dispersion) perpendicular to the cleavage plane,¹³ with an anisotropic

dispersion of about 1 eV in the In chain direction.¹² In spite of all these known details of the band structure, to the best of our knowledge neither experimental data (with the exception of far-infrared optical properties¹⁵⁻¹⁷) nor theoretical calculations of wide range optical spectra of the In_4Se_3 are available in the literature. Therefore, and since state-of-the-art calculations have sensibly improved, an exhaustive and updated theoretical study of the In_4Se_3 optical properties based on *ab initio* calculations is quite desirable.

In this work, we present a thorough study of the optical properties of the system: the dielectric function—real and imaginary parts, the complex refractive index, the reflectivity, the absorption coefficient, and the conductivity of In_4Se_3 were calculated with the inclusion of the spin-orbit interaction. Based on our previous electronic structure results,^{12,14} we discuss the location and nature of the main optical peaks appearing in the spectra. As a companion to the theory, we report the determination of the intrinsic orthorhombic optical properties for photon energies from 0.76 to 3.1 eV of In_4Se_3 single crystals cut approximately parallel to (100). Biaxial optical properties of anisotropic bulk and thin film materials can be obtained by generalized ellipsometry. This concept has been demonstrated recently for numerous materials, and particularly for the orthorhombic,¹⁸⁻²⁰ monoclinic,^{21,22} and triclinic²³ materials. Our experimental results show a good agreement with our calculations.

We obtained optical properties with rather anisotropic behavior, mainly in the infrared-visible region, which can be explained with our model. Our results predict the optical properties on this system, to much higher energies than currently available from experiment.

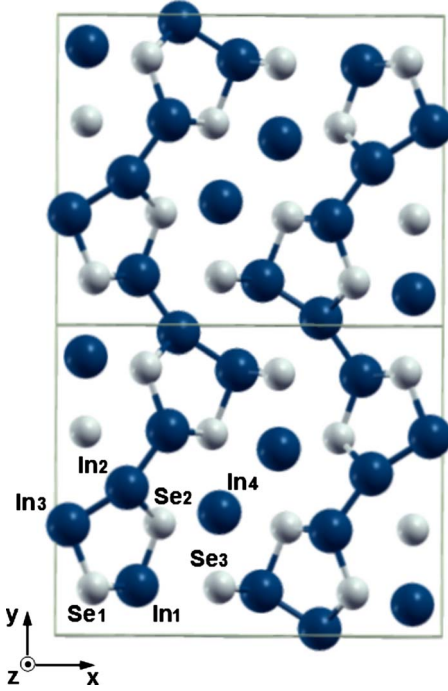


FIG. 1. (Color online) Two unit cells of In_4Se_3 . The axes x , y , and z correspond to the lattice parameters (Ref. 12) $a=15.297(1)$, $b=12.308(1)$, and $c=4.0810(5)$, respectively. The cleavage is perpendicular to axis x . The seven inequivalent atoms are labeled in the lower unit cell.

II. COMPUTATIONAL DETAILS

A. Method

We modeled the In_4Se_3 in the framework of the density functional theory (DFT),^{24–26} using a full potential linearized augmented plane-wave (FP-LAPW) method.^{27–33} In this work, we used the WIEN2K package,³⁴ which self-consistently finds the eigenvalues and eigenfunctions of the Kohn-Sham³⁵ equations for the system. As it is well known the local density approximation (LDA) (e.g., in the Perdew-Wang parametrization³⁶) for the exchange and correlation potential has had great success in dealing with the calculation of electronic properties. However, it does not accurately describe some important properties, for example, there is a tendency to underestimate the band gaps. A formal correction is achieved by including the gradient of the charge density. This is the so-called generalized gradient approximation (GGA),³⁷ which we used in the formal Engel-Vosko scheme.³⁸ We also tested the Perdew-Burke-Ernzerhof (PBE) parametrization scheme,^{39–41} but found, similarly to other authors,^{42,43} that the Engel-Vosko scheme gives improved results of the band gap, so we present here only these latter. However, we present in Table I our band gaps both with PBE and EV-GGA scheme, along with other reported in the literature. All these schemes usually underestimate the band gap. A common correction of this underestimation is the scissors operator,⁴⁶ which can be used even when some non-rigid shifts of bands occur in semiconductors, provided that the k dependence of the error in the excitation energies is negligible. In particular, this approximation is often used in the

TABLE I. Our calculated band gaps (in eV) in comparison with other calculations and experiment.

	Our cal.		Other calc.	
	GGA-PBE	GGA-EV	LDA	Expt.
With SO	0.32	0.57		0.65 ^b
Without SO	0.32	0.58	~ 0.3 ^a	

^aReference 11.

^bReferences 44 and 45.

determination of the band gap offsets^{47,48} in considering interfaces between different semiconductors, and also when optical transitions are studied.^{49,50} Even though there are formal theoretical improvements like the GW and BSE methods,^{51–55} these are still applied in solids using the k -independent scissors approximation due to its good performance and also to maintain the volume of calculations in a tractable way.^{53–55} Time-dependent DFT (TDDFT) (Ref. 56) is also making progress in non-linear optical properties such as those shown under the incidence of “strong” laser beams⁵⁷ or ultrafast phenomena in semiconductors.⁵⁸ We have not used the scissors operator since our electronic structure calculations reproduce quite well the experimental band structure¹² and our band gap is comparable to those reported in the literature.

B. Self-consistent electronic structure

The calculation of optical properties begins with a self-consistent electronic structure. This is a key requisite since the calculation of optical properties involves matrix elements from the momentum operator, and the eigenfunctions used in their calculation must be precise. We used 120 irreducible k points in the BZ for the self-consistent calculation, with a $R_{MT}K_{max}$ product of 7. Here R_{MT} is the smallest of all atomic sphere radii and K_{max} is the plane-wave cutoff. The system has 28 (i.e., 7 times 4) atoms in the unit cell with seven crystallographically inequivalent sites (four indium and three selenium), each of which occupying four equivalent positions.

C. Optical properties

From our electronic structure calculations, we determined the imaginary part, $\varepsilon_2(\omega)$, of the complex dielectric function, $\varepsilon(\omega)$, integrating in k space (by the standard tetrahedron method⁵⁹). The general expression for the complex dielectric tensor is⁶⁰

$$\varepsilon_2(\omega)_{\alpha\beta} = \frac{4\pi^2 e^2}{m^2 \omega^2} \sum_{i,f} \int \langle f|p_\alpha|i\rangle \langle f|p_\beta|i\rangle \times W_i(1 - W_f) \delta(E_f - E_i - \hbar\omega) d^3k, \quad (1)$$

where $\langle f|p_\alpha|i\rangle$ and $\langle f|p_\beta|i\rangle$ are the dipole matrix elements corresponding to the α and β directions of the crystal (x , y , or z), and f and i , are the final and initial states, respectively, W_n and E_n are the Fermi distribution function and

electron energy for the n th state, respectively. The real part of the diagonal dielectric functions is computed from $\epsilon_2(\omega)$ using the Kramers-Kronig relations in the form

$$\epsilon_1(\omega)_{\alpha\alpha} = 1 + \frac{2}{\pi} P \int_0^{\infty} \frac{\omega' \epsilon_2(\omega')_{\alpha\alpha}}{\omega'^2 - \omega^2} d\omega', \quad (2)$$

where P means the principal value of the integral. In order to give a complete discussion of the optical spectra of In_4Se_3 , we also studied the real and imaginary parts of the complex refraction index $\tilde{n}(\omega)_{\alpha\alpha} = n(\omega)_{\alpha\alpha} + ik(\omega)_{\alpha\alpha}$, where $n(\omega)$ is the ordinary refraction index and $k(\omega)$ is the coefficient of extinction, obtained from $[\tilde{n}(\omega)_{\alpha\alpha}]^2 = \epsilon_1(\omega)_{\alpha\alpha} + i\epsilon_2(\omega)_{\alpha\alpha}$. Finally, we also computed the reflectivity according to

$$R(\omega) = \left| \frac{1 - \tilde{n}(\omega)_{\alpha\alpha}^*}{1 + \tilde{n}(\omega)_{\alpha\alpha}^*} \right|^2 \quad (3)$$

where $*$ means conjugate complex, the coefficient of absorption,

$$\alpha(\omega)_{\alpha\alpha} = \frac{2\omega}{c} \left(\frac{-\epsilon_1(\omega)_{\alpha\alpha} + |\epsilon(\omega)_{\alpha\alpha}|}{2} \right)^{1/2} = \frac{2\omega}{c} k(\omega)_{\alpha\alpha} \quad (4)$$

and the conductivity using

$$\text{Re} = \frac{\omega}{4\pi} \text{Im}[\epsilon(\omega)_{\alpha\alpha}] = \frac{\omega}{4\pi} \epsilon_2(\omega)_{\alpha\alpha}. \quad (5)$$

Our calculations, based on a ground state scheme as DFT, could imply inaccuracies due to the omission of the local-field correction and the electron-hole interaction. In order to improve these inaccuracies, new techniques capable of incorporating them to the absorption spectra description (still built upon the DFT framework) are being developed.^{49,52,61–63} In spite of those inaccuracies we found good agreement between theory and experiment, which suggests that those non-linear effects are not of importance of In_4Se_3 . This requires further confirmation by further theoretical and experimental studies. More sophisticated approaches to the theory than DFT and extending the energy range of the experimental measurements are likely to prove valuable.

III. EXPERIMENTAL DESCRIPTION AND ANALYSIS

Generalized ellipsometry allows for determination of the optical constants or alternatively dielectric constants for biaxial (dielectrically anisotropic) materials. For arbitrarily anisotropic materials, the complex ratio ρ of the s - and p -polarized reflectivities depends on the polarization state of the incident light. Measurement of ρ can be addressed within different presentations of the electromagnetic plane-wave response. Here we made use of the Stokes descriptive system. Real-valued Mueller matrix elements M_{ij} connect the Stokes parameters before and after sample interaction.^{64,65} The Stokes vector elements for the traditional p - s polarization system are: $S_0 = I_p + I_s$, $S_1 = I_p - I_s$, $S_2 = I_{45} - I_{-45}$, $S_3 = I_{\sigma^-} - I_{\sigma^+}$, where I_p , I_s , I_{45} , I_{-45} , I_{σ^-} , I_{σ^+} denote the intensities for the p , s , $+45^\circ$, -45° , right-, and left-handed circularly polarized light components, respectively. Data analysis requires non-linear regression methods, where measured and calculated

generalized ellipsometry data were matched as closely as possible by varying appropriate physical model parameters. The data analysis require the setup of models for geometry (sample crystal axes orientation), and polarizability properties of the materials involved in the sample of interest.

For orthorhombic materials the major dielectric function values ϵ_{xx} , ϵ_{yy} , and ϵ_{zz} for polarization along crystal axes a , b , and c , respectively, and Euler angle coordinates φ , ψ , and θ provide a complete description of the dielectric function tensor ϵ within the laboratory frame of reference, as defined in Eq. (12) of Ref. 66 and in Fig. 1 of Ref. 67. In this work, the so-called wavelength-by-wavelength data inversion method was employed, i.e., in addition to model parameters φ , ψ , and θ constant for all wavelengths, function values ϵ_{xx} , ϵ_{yy} , and ϵ_{zz} were obtained at each wavelength independent from spectrally adjacent wavelengths. Thereby, no *a priori* physical line shape model was implemented into our model analysis schemes, allowing for model unbiased extraction of intrinsic dielectric function values ϵ_{xx} , ϵ_{yy} , and ϵ_{zz} .

The angle-resolved (angle of incidence Φ_A and in-plane rotation angle φ) spectroscopic Mueller matrix ellipsometry measurements were performed using a commercial instrument (M2000, J. A. Woollam Co., Inc.) within a spectral range from 0.76 to 3.1 eV. A near (100) surface of single crystal In_4Se_3 with a -axis orientation approximately 7° off away from the surface normal was measured. The ellipsometer was mounted on an automatic variable Φ_A and sample rotator φ stage. Φ_A was varied from 45° to 75° in steps of 10° , while φ was varied from 0° to 360° in steps of 5° . The polarizer-compensator-sample-analyzer ellipsometer is capable of measuring 11 out of 16 Mueller matrix elements normalized to M_{11} (except for elements in fourth row).⁶⁴ Figures 2 and 3 depict experimental and best-match model calculated data at selected wavelengths, angles of incidence and sample azimuth rotations. Given the fact that In_4Se_3 is a corrugated but otherwise layered compound with an easy cleavage parallel to (100) planes (i.e., perpendicular to the a -axis), there are difficulties in preparing a high quality surface parallel to the a -axis, i.e., $\langle 100 \rangle$ direction or cleavage plane normal. These, in term, result in off axis ellipsometry data insufficiently reliable for comparison of the experiment with theory for ϵ_{xx} . We have therefore restricted our comparison between experiment and theory for the real and imaginary parts of the dielectric functions extracted along the $\langle 010 \rangle$ and $\langle 001 \rangle$ directions (i.e., ϵ_{yy} and ϵ_{zz}), which we discuss in Sec. IV B.

IV. DISCUSSION OF RESULTS

A. Band structure and DOS

Figure 4 shows the energy band structure with spin-orbit (SO) interaction—which is almost identical to those without, while Figs. 5–7 show several DOS.

The electronic structure of In_4Se_3 without spin-orbit can be understood as four main bundles of valence bands and two of conduction bands (see Fig. 4 and specially bottom floor of Fig. 5). There is a flat isotropic band between -15.30 and -14.25 eV, mostly due to the $\text{In } d$ orbitals and a much lesser contribution of $\text{Se } s$ states. This band is followed by a

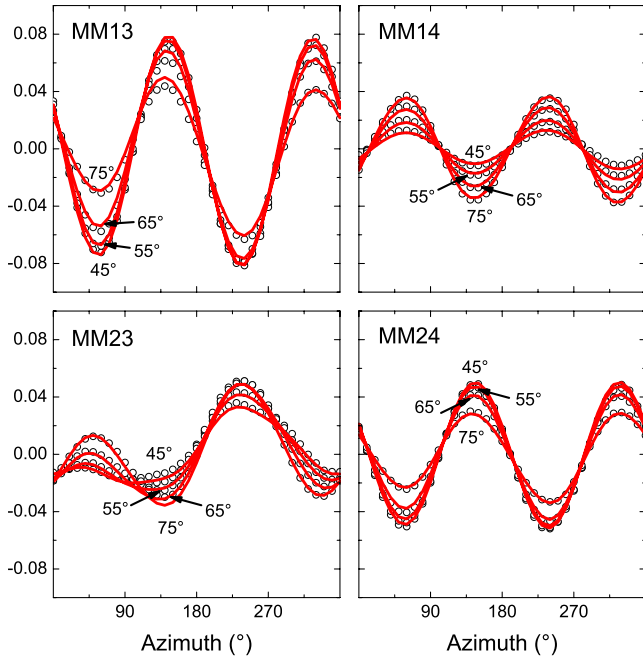


FIG. 2. (Color online) Selected experimental (symbols) and best-match model calculated GE data M_{13} , M_{14} , M_{23} , M_{24} versus sample azimuth rotation, at photon energy 2.1 eV, and various angle of incidence ($\Psi_a=45^\circ, 55^\circ, 65^\circ, 75^\circ$).

less populated d_i band resulting from Se s but also from the In d orbitals (though with a less significant contribution) between -13.50 and -11.90 eV binding energies. Then there is an empty (unoccupied) region between -11.90 and -6.83 eV below the Fermi level, where the bottom of the

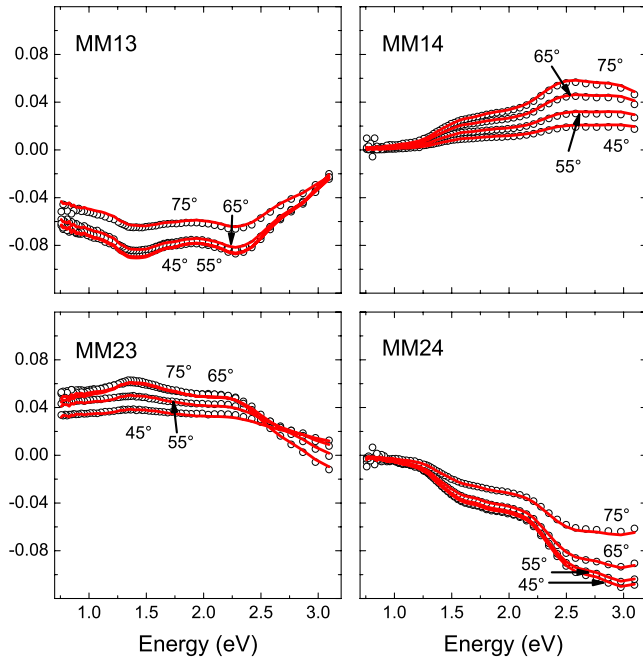


FIG. 3. (Color online) Selected experimental (symbols) and best-match model calculated GE data M_{13} , M_{14} , M_{23} , M_{24} , versus photon energy at sample azimuth rotation 240° , and angle of incidence ($\Psi_a=45^\circ, 55^\circ, 65^\circ, 75^\circ$).

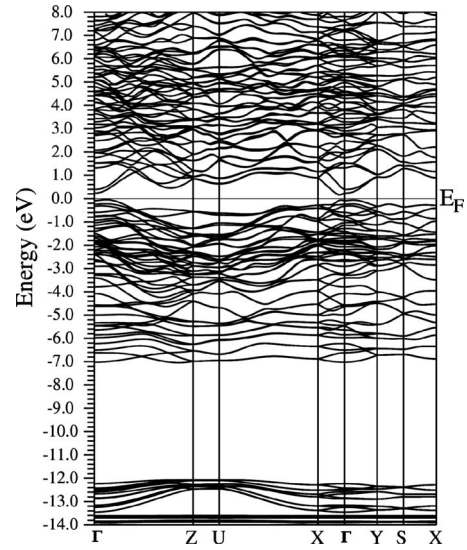


FIG. 4. Band structure with the inclusion of the spin orbit interaction, calculated with the Engel–Vosko GGA.

valence band begins. At the bottom of the valence, we find four noticeable peaks (A-D in Fig. 5) due to similar contributions from In s and Se p electrons. The whole valence band is mostly formed by Se p electrons, except for energies above 5.00 eV where In s predominates (peaks A and B). The bands between -5.26 and -4.04 eV have equal contributions from In s and Se p orbitals. The bands above -4.04 eV are mostly formed by Se p electrons. As general observation, we note that crystallographically each of the nonequivalent Se atoms contribute an almost identical density of state (see second panel of Fig. 5). In contrast, In atoms show some differences, especially In4 atoms (see peaks C_{In} and F_{In} in the top panel of Fig. 5) with respect to the other In atoms.

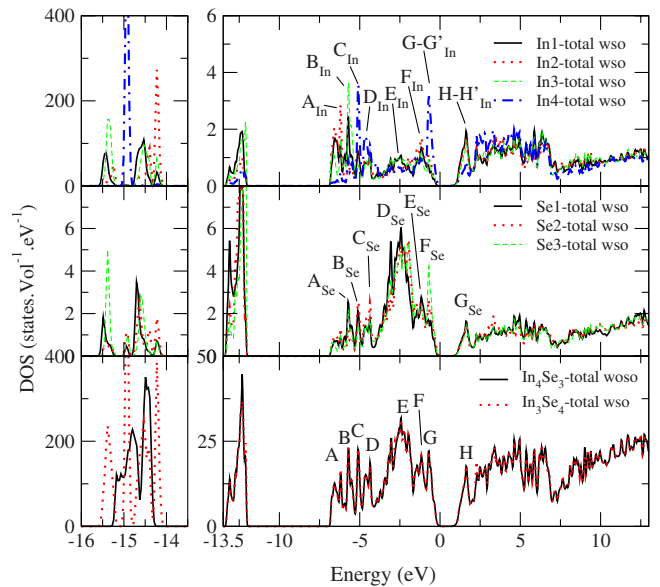


FIG. 5. (Color online) Total DOS of the seven inequivalent atoms of the unit cell and (see bottom floor) comparison of the total DOS for the whole system with against without the inclusion of spin-orbit. wso: with SO, woso: without SO.

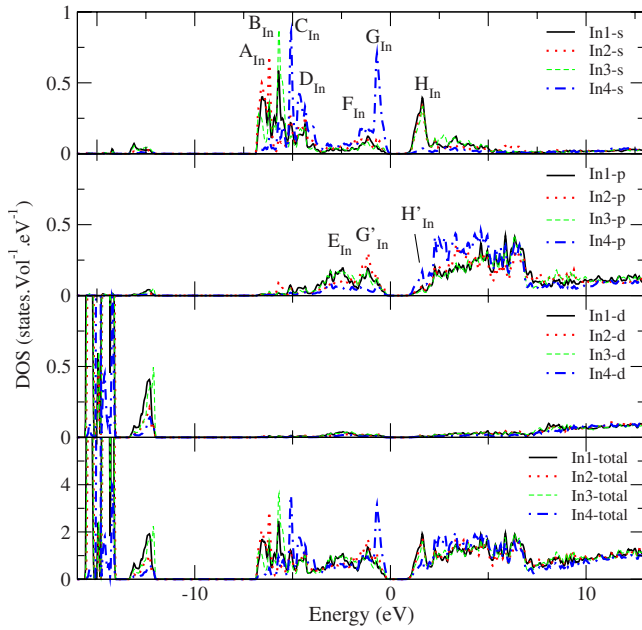


FIG. 6. (Color online) Orbital-resolved DOS of the four inequivalent atoms of Indium.

The conduction band is mainly p -like (with both In and Se contributions). However, there is a sharp peak in the DOS due to the In s orbitals near the bottom of the conduction band. A similar situation holds for the narrow In4 $4s$ states near the valence band maximum. These s -cation states, hybridized with their p -cation and -anion counterparts, are very important for the physical properties of this material, since they define the band gap. The band gaps with and without spin-orbit are almost the same: 0.57 and 0.58 eV, respectively, both of them direct at Γ . Further, the morphology of the bands with and without spin-orbit is almost identical (see

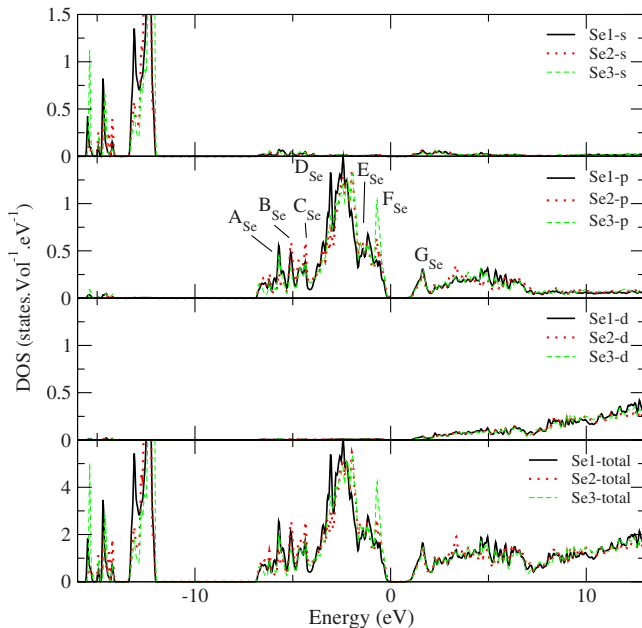


FIG. 7. (Color online) Orbital-resolved DOS of the three inequivalent atoms of Selenium.

TABLE II. Approximated location (E) of main total DOS structures (labeled A to H, bottom floor of Fig. 5) and its component, atom- and orbital-resolved.

DOS peaks	E (eV)	Main atomic contributions
A	-6.35	A_{In} (In2 s , In1 s , In3 s)
B	-5.69	B_{In} (In3 s , In1 s , In4 s) A_{Se} (Se1 p , Se3 p)
C	-5.07	C_{In} (In4 s) B_{Se} (Se2 p , Se1 p , Se3 p)
D	-4.44	D_{In} (In4 s , In2 s , In3 s , In1 s) C_{Se} (Se2 p , Se3 p , Se1 p)
E	-2.49	D_{Se} (Se p) E_{In} (In1 p In3 p)
F	-1.31	E_{Se} (Se p), E_{In} (In s) G_{In} (In2 p , In1 p , In3 p) F_{In} (In4 s)
G	-0.67	F_{Se} (Se1 p , Se2 p , Se1 p) G_{In} (In4 s), G_{In} (In2 p , In1 p , In3 p)
H	1.64	H_{In} (In1 s , In2 s , In3 s), H_{In} (In4 p) G_{Se} (Se p)

also comparison of the DOS in the bottom panel of Fig. 5), except for minor splittings of the band all over the BZ. There is however a strong and noticeable splitting of the bands around -15 eV into four sharply defined bands. Table II shows the approximate location of the main structures of the total DOS, as well as the most important contributions to them, atomic and orbital resolved.

B. Optical properties

In order to assess convergence of the optical properties, we calculated ϵ_2 with increasingly finer meshes for the discretization of the BZ: 144, 192, and 300 k points without the spin-orbit (SO) interaction, and 144 k points with it. All of them were coincident, therefore, we assume convergence at 144 k points and report all optical spectra with spin orbit. All the calculated optical spectra are presented in Fig. 8 (ϵ_1 , ϵ_2 , n , and k) and Fig. 9 (R , α , and σ), and the location (in energy) of their main structures is tabulated in Tables III and IV. It can be seen in all spectra that the material has a triaxial anisotropy for energies up to ~ 1.5 eV, and a quasi-2D behavior for higher energies, since curves for the x and y axes are very similar (though not identical), while those for the z axis are clearly different (in amplitude and/or shape). Finally, we note that isotropy only appears in small isolated energy ranges above 15 eV.

Dispersion. The real part of the dielectric function (ϵ_1) is closely related to the dispersion of incident photons by the material, so is the refractive index (n), and in a less obvious way is the reflectivity (that actually results from the combination of absorption and dispersion), which are presented in Fig. 8 (ϵ_1 and n) and 9 (R). It can be seen that n_{xx} has its main peak (1_x) coinciding with that of n_{yy} (0_y) at 1.84 eV. In

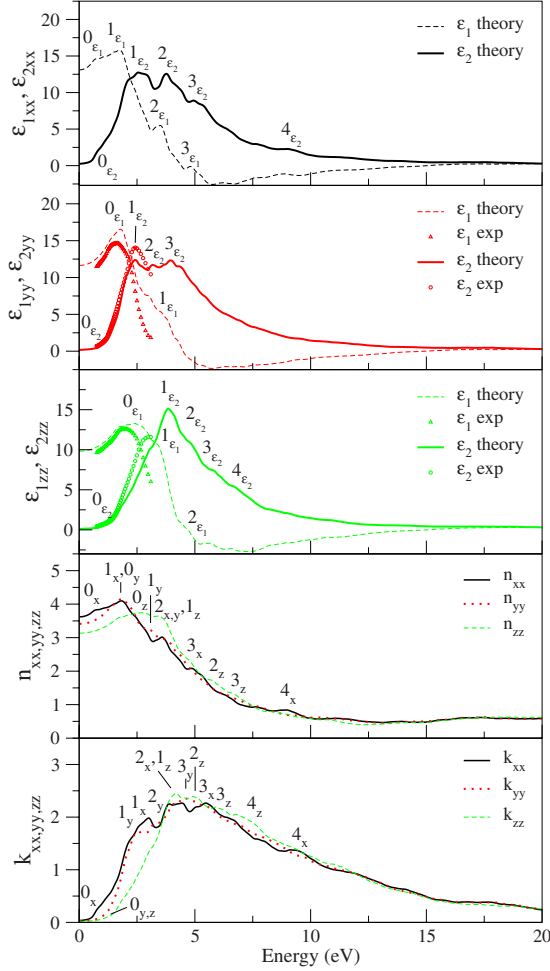


FIG. 8. (Color online) Top to bottom floors: real (ϵ_1) and imaginary (ϵ_2) part of the dielectric function comparing with experiment for yy and zz axes-, index of refraction (n) and coefficient of extinction (k). The position (in eV) of the labeled peaks is in Table III.

fact both indexes coincide almost exactly in the range from ~ 1.3 to 3.0 eV and also for $E \sim 3.5$ eV, i.e., the material is birefringent in the near IR-visible and also from the UVB up in the spectrum. It shows, however, a triaxial behavior in the range 3.0 – 3.5 eV (blue to UVA range). As to n_{zz} it shows a blunt plateau rather than a pronounced peak. The real part of ϵ follows closely the morphology of n , and for yy and zz axes we also present ellipsometry measurements showing excellent agreement with theory for energies up to ~ 2.0 eV. While there is a faster drop of the remaining experimental points for higher energies, up to 3.1 . With respect to the reflectivity, it oscillates between $\sim 30\%$ and $\sim 50\%$ for incident energies up to ~ 12.5 eV, where it drops sensibly. In addition, it is to be noticed that reflectivity shows strong anisotropy for energies above 7.5 eV while in the other properties, anisotropy apparently decreases: reflectivity just enhances the effect of what in other properties appears as small differences among the different axes.

Energy intake. The imaginary part of the dielectric function (ϵ_2) is closely related to the intake of energy by the material, and so are the coefficients of extinction (k) and absorption (α), and the optical conductivity (σ), which are

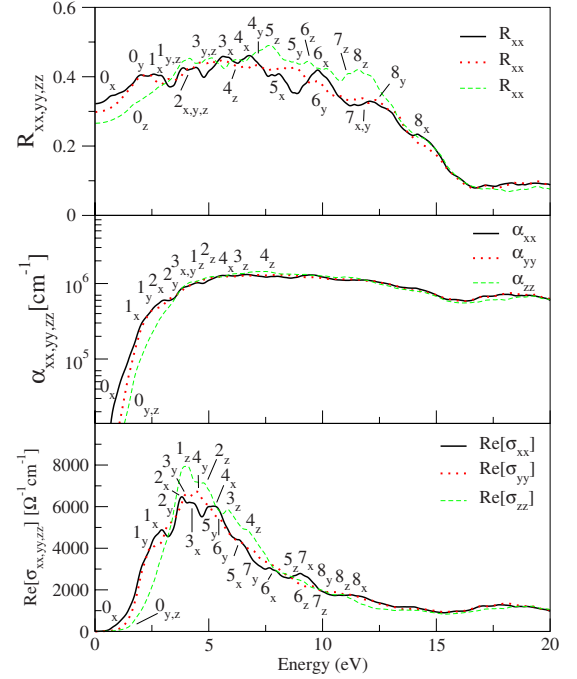


FIG. 9. (Color online) Reflectivity (R), absorption coefficient (α) and real part of the diagonal elements of the optical conductivity tensor ($\text{Re}[\sigma]$). The position (in eV) of the labeled peaks is in Table IV.

presented in Figs. 8 (ϵ_2 and k) and 9 (α and σ). The general similarity of all these properties is clear: they have a gap at low energy (which is the optical manifestation of the electronic band gap), after which they rise, have some complicated fine structure, and then decay as photon energies increase ($E_{ph} \geq 5$ eV). In all of them the property for the x axis

TABLE III. Values at $E=0$ and approximate positions (in eV) of main peaks of the optical properties of In_4Se_3 .

Peaks	ϵ_1			ϵ_2		
	x	y	z	x	y	z
$\epsilon_{1E=0}$	13.04	11.61	9.87			
0	0.70	1.79	2.31	0.58	1.06	1.42
1	1.75	3.79	3.37	2.58	2.45	3.87
2	3.50		4.64	3.77	3.20	4.83
3	4.85			5.19	3.98	5.81
4				9.13		6.71
Peaks	n			k		
	x	y	z	x	y	z
$n_{E=0}$	3.62	3.41	3.14			
0	0.69	1.91	2.67	0.62	1.19	1.43
1	1.84	3.06	3.52	3.02	2.48	4.19
2	3.61	3.70	5.76	4.18	3.30	4.98
3	4.94		6.69	5.46	4.73	6.06
4	9.02			9.41		7.26

TABLE IV. Values at E=0 and approximate positions (in eV) of main peaks of the optical properties of In₄Se₃.

Peaks	α			R			$\text{Re}[\sigma]$		
	x	y	z	x	y	z	x	y	z
$R_{E=0}$				0.32	0.30	0.27			
1	0.72	1.10	1.30	0.58	2.23	1.79	0.64	1.16	1.51
2	2.98	3.29	5.15	3.28	4.01	4.10	3.85	3.27	4.79
3	3.90	4.03	6.21	4.49	5.11	5.11	4.25	4.00	5.84
4	5.60		7.34	5.47	7.18	6.16	5.24	4.44	6.69
5				6.53	8.61	7.69	6.33	5.01	8.30
6				7.85	9.84	9.36	7.80	5.44	9.04
7				9.75	11.76	10.27	9.07	7.00	9.82
8				11.35	12.40	11.53	11.38	9.57	10.86

risers first (i.e., for a lower energy, see 0_x in Tables III and IV) followed by the other two axes almost together (0_y and 0_z). They, however, separate from each other from ~ 1.5 eV on since the spectra for photons polarized in the z direction grow slower. Indeed, the first and only peak of for instance ε_{2zz} (2_z), is shifted upward in energy and almost coincides with the second peak of the other two curves (ε_{2xx} and ε_{2yy}). The peak 1_z (3.02 eV) seems to be due to the transition $F \rightarrow H$ [$1.64 - (-1.31) = 2.95 \sim 3.02$]. We also present experimental curves for ε_2 in the range from 0.76 to 3.1 eV for the b - and c -axes. As for ε_1 , the agreement between theory and experiment is excellent up to ~ 2.0 eV (e.g., for ε_{yy} theory and experiment coincide exactly). For higher energies the experimental ε_{zz} rise faster, while the experimental ε_{yy} overshoots our calculations, which still correctly predict the energy location of peak 1_{e_2} (see Fig. 8).

V. CONCLUSIONS

We have performed what to the best of our knowledge is the first computational analysis of the optical properties of

the binary compound In₄Se₃. We also performed ellipsometry measurements and determined the real and imaginary parts of the dielectric function, finding good agreement with the theoretical results. Given the scarce availability of experimental measurements on the system, our spectra result rather predictive, showing bi- and triaxial anisotropy for different ranges of incident photon energy. We highlight the importance of our calculations for the xx axis, since measurements in that direction face serious experimental difficulties.

ACKNOWLEDGMENTS

L.M., E.A.A., and N.V.G.L. acknowledge financial support from the Consejo Nacional de Investigaciones Científicas y Técnicas (CONICET), the Universidad Nacional de Entre Ríos (UNER) Argentina, and the Agencia de Promoción Científica y Tecnológica (ANPCyT). D.S., M.S. and E.S. acknowledge support in part from NSF SGER ECCS-0824920, CAREER ECCS-0846329, DMR-0907475, MRI DMR-0922937, MRSEC QSPIN DMR-0820521, and J.A. Woollam Foundation.

*Author to whom correspondence should be addressed; lmakinistian@santafe-conicet.gov.ar

¹U. Schwarz, H. Hillebrecht, H. Deiseroth, and R. Walther, Z. Kristallogr. **210**, 342 (1995).

²W. Jaegermann, A. Klein, and C. Pettenkofer, *Physics and Chemistry of Materials with Low-Dimensional Structures*, edited by H. P. Hughes and H. I. Starnberg (Kluwer Academic Publishers, Dordrecht, 2000), Vol. 24, pp. 317–402.

³O. Balitskii, V. Savchyn, B. Jaeckel, and W. Jaegermann, Physica E **22**, 921 (2004).

⁴T. Gertovich, S. Grineva, B. Gritsiuk, A. Ogorodnika, O. Stoliarchuk, and K. Tovstiuk, Ukr. Fiz. Zh. (Russ. Ed.) **27**, 1191 (1982).

⁵P. Galiy, T. Nenchuk, O. Dveriy, A. Ciszewski, P. Mazur, and S. Zuber, Physica E **41**, 465 (2009).

⁶J. Rhyee, K. H. Lee, S. Lee, E. Cho, S. Kim, E. Lee, Y. Kwona, J. Shim, and G. Kotliar, Nature (London) **459**, 965 (2009).

⁷N. Benramdane and R. Musho, Sol. Energy Mater. Sol. Cells **37**, 367 (1995).

⁸T. Melnychuk, V. Strebegev, and G. Vorobets, Appl. Surf. Sci. **254**, 1002 (2007).

⁹P. Galiy, T. Nenchuk, J. Stakhira, and Y. Fiyala, J. Electron Spectrosc. Relat. Phenom. **105**, 91 (1999).

¹⁰D. Bercha and K. Rushchanski, Phys. Solid State **40**, 1906 (1998).

¹¹M. Sznajder, K. Rushchanskii, L. Kharkhalis, and D. Bercha, Phys. Status Solidi B **243**, 592 (2006), and references therein.

¹²Y. B. Losovyj, M. Klinke, E. Cai, I. Rodriguez, J. Zhang, L. Makinistian, A. G. Petukhov, E. A. Albanesi, P. Galiy, Y. Fiyala, Jing Liu, and P. A. Dowben, Appl. Phys. Lett. **92**, 122107 (2008).

¹³J. Liu, Y. Losovyj, T. Komesu, P. Dowben, L. Makinistian, E. Albanesi, A. Petukhov, P. Galiy, and Y. Fiyala, Appl. Surf. Sci. **254**, 4322 (2008).

- ¹⁴Y. B. Losovyj, L. Makinistian, E. A. Albanesi, A. G. Petukhov, J. Liu, P. Galij, O. R. Dveriy, and P. A. Dowben, *J. Appl. Phys.* **104**, 083713 (2008).
- ¹⁵V. P. Zakharov, V. P. Savchin, I. M. Stakhira, and G. P. Sheremet, *Sov. Phys. Solid State* **23**, 1101 (1981).
- ¹⁶O. Madellung, *Semiconductors: Data Handbook*, 3rd ed. (Springer, New York, 2004).
- ¹⁷C. Julien, M. Eddrief, M. Balkanski, and A. Chevy, *Phys. Rev. B* **46**, 2435 (1992).
- ¹⁸M. Schubert, *Ann. Phys.* **15**, 480 (2006).
- ¹⁹M. Schubert and W. Dollase, *Opt. Lett.* **27**, 2073 (2002).
- ²⁰M. Schubert, T. Hofmann, C. M. Herzinger, and W. Dollase, *Thin Solid Films* **455-456**, 619 (2004).
- ²¹D. Schmidt, B. Booso, T. Hofmann, E. Schubert, A. Sarangan, and M. Schubert, *Appl. Phys. Lett.* **94**, 011914 (2009).
- ²²D. Schmidt, B. Booso, T. Hofmann, E. Schubert, A. Sarangan, and M. Schubert, *Opt. Lett.* **34**, 992 (2009).
- ²³M. Dressel, B. Gompf, D. Faltermeier, A. K. Tripathi, J. Pflaum, and M. Schubert, *Opt. Express* **16**, 19770 (2008).
- ²⁴L. Thomas, *Proc. Cambridge Philos. Soc.* **23**, 542 (1927).
- ²⁵E. Fermi, *Z. Phys.* **48**, 73 (1928).
- ²⁶P. Hohenberg and W. Kohn, *Phys. Rev.* **136**, B864 (1964).
- ²⁷D. Koelling and G. Arbman, *J. Phys. F: Met. Phys.* **5**, 2041 (1975).
- ²⁸O. K. Andersen, *Phys. Rev. B* **12**, 3060 (1975).
- ²⁹O. Jepsen, J. Madsen, and O. K. Andersen, *Phys. Rev. B* **26**, 2790 (1982).
- ³⁰M. Weinert, E. Wimmer, and A. Freeman, *Phys. Rev. B* **26**, 4571 (1982).
- ³¹H. Jansen and A. Freeman, *Phys. Rev. B* **30**, 561 (1984).
- ³²L. Mattheiss and D. Hamann, *Phys. Rev. B* **33**, 823 (1986).
- ³³S. Cottenier, *Density Functional Theory and the Family of (L)APW-Methods: A Step-by-Step Introduction* (Instituut voor Kern-en Stralingsfysica, K.U. Leuven, Belgium, 2002).
- ³⁴K. Schwarz, P. Blaha, and G. K. H. Madsen, *Comput. Phys. Commun.* **147**, 71 (2002).
- ³⁵W. Kohn and L. Sham, *Phys. Rev.* **140**, A1133 (1965).
- ³⁶J. P. Perdew and Y. Wang, *Phys. Rev. B* **45**, 13244 (1992).
- ³⁷J. P. Perdew, J. A. Chevary, S. H. Vosko, K. A. Jackson, M. R. Pederson, D. J. Singh, and C. Fiolhais, *Phys. Rev. B* **46**, 6671 (1992).
- ³⁸E. Engel and S. H. Vosko, *Phys. Rev. B* **47**, 13164 (1993); **50**, 10498 (1994).
- ³⁹J. P. Perdew, K. Burke, and M. Ernzerhof, *Phys. Rev. Lett.* **77**, 3865 (1996).
- ⁴⁰J. P. Perdew, K. Burke, and M. Ernzerhof, *Phys. Rev. Lett.* **78**, 1396 (1997).
- ⁴¹J. Perdew, S. Kurth, A. Zupan, and P. Blaha, *Phys. Rev. Lett.* **82**, 2544 (1999).
- ⁴²S. Drablia, H. Meradji, S. Ghemid, S. Labidi, and B. Bouhafas, *Phys. Scr.* **79**, 045002 (2009).
- ⁴³M. Dadsetani and A. Pourghazi, *Opt. Commun.* **266**, 562 (2006).
- ⁴⁴V. P. Savchin, *Fiz. Tekh. Poluprovodn.* **15**, 1430 (1981) [*Sov. Phys. Semicond.* **15**, 827 (1981)].
- ⁴⁵D. Bercha, A. Borets, I. Stakhira, and K. Towstyuk, *Phys. Status Solidi* **21**, 769 (1967).
- ⁴⁶R. Del Sole and R. Girlanda, *Phys. Rev. B* **48**, 11789 (1993).
- ⁴⁷S. H. Wei and A. Zunger, *Phys. Rev. B* **55**, 13605 (1997).
- ⁴⁸E. A. Albanesi, W. L. Lambrecht, and B. Segall, *J. Vac. Sci. Technol. B* **12**, 2470 (1994).
- ⁴⁹R. Laskowski, N. E. Christensen, G. Santi, and C. Ambrosch-Draxl, *Phys. Rev. B* **72**, 035204 (2005).
- ⁵⁰K. Stahrenberg, T. Herrmann, K. Wilmers, N. Esser, W. Richter, and M. J. G. Lee, *Phys. Rev. B* **64**, 115111 (2001).
- ⁵¹Z. H. Levine and C. Allan, *Phys. Rev. Lett.* **63**, 1719 (1989).
- ⁵²G. Onida, L. Reining, and A. Rubio, *Rev. Mod. Phys.* **74**, 601 (2002).
- ⁵³B. Arnaud and M. Alouani, *Phys. Rev. B* **63**, 085208 (2001); **62**, 4464 (2000).
- ⁵⁴K. Hummer and C. Ambrosch-Draxl, *Phys. Rev. B* **71**, 081202(R) (2005).
- ⁵⁵F. Ladstädter, U. Hohenester, P. Puschnig, and C. Ambrosch-Draxl, *Phys. Rev. B* **70**, 235125 (2004).
- ⁵⁶K. Burke, J. Wershenik, and E. K. U. Gross, *J. Chem. Phys.* **123**, 062206 (2005).
- ⁵⁷M. A. L. Marques and E. K. U. Gross, *Annu. Rev. Phys. Chem.* **55**, 427 (2004).
- ⁵⁸V. Turkowski and C. A. Ullrich, *Phys. Rev. B* **77**, 075204 (2008).
- ⁵⁹P. E. Blöchl, O. Jepsen, and O. K. Andersen, *Phys. Rev. B* **49**, 16223 (1994).
- ⁶⁰C. Ambrosch-Draxl and J. O. Sofo, *Comput. Phys. Commun.* **175**, 1 (2006).
- ⁶¹S. Baroni, S. de Gironcoli, A. D. Corso, and P. Giannozzi, *Rev. Mod. Phys.* **73**, 515 (2001).
- ⁶²K. Hummer, C. Ambrosch-Draxl, G. Bussi, A. Ruini, M. J. Caldas, E. Molinari, R. Laskowski, and N. E. Christensen, *Phys. Status Solidi* **242**, 1754 (2005) b.
- ⁶³L. Hedin, in *Solid State Physics*, edited by H. Ehrenreich, F. Seitz, and D. Turnbull (Academic Press, New York, 1969), Vol. 23, p. 1.
- ⁶⁴L. Hedin, *Phys. Rev.* **139**, A796 (1965); *Handbook of Ellipsometry*, edited by H. G. Tompkins and E. A. Irene (Springer, New York, 2004).
- ⁶⁵H. Fujiwara, *Spectroscopic Ellipsometry: Principles and Applications* (Wiley, New York, 2007).
- ⁶⁶M. Schubert, *Phys. Rev. B* **53**, 4265 (1996).
- ⁶⁷M. Schubert and C. M. Herzinger, *Phys. Status Solidi A* **188**, 1563 (2001), the following correction should be made to page 1566: $A^{-1}(\varphi, \psi, \theta) = A^T(\varphi, \psi, \theta)$ where T is the transpose of A .